



## Research paper

## Investigating the barrier function of skin lipid models with varying compositions

Daniël Groen, Dana S. Poole, Gert S. Gooris, Joke A. Bouwstra\*

Leiden/Amsterdam Center for Drug Research, Department of Drug Delivery Technology, University of Leiden, Leiden, The Netherlands

## ARTICLE INFO

## Article history:

Received 24 November 2010

Accepted in revised form 23 May 2011

Available online 30 May 2011

## Keywords:

Skin

Lipids

Stratum corneum

Model

In vitro

Permeation

## ABSTRACT

The lipids in the uppermost layer of the skin, the stratum corneum (SC), play an important role in the barrier function. The main lipid classes in stratum corneum are ceramides, cholesterol, and free fatty acids. In previous publications, a lipid model was presented, referred to as the stratum corneum substitute (SCS), that closely mimics the SC lipid organization and SC barrier function. In the present study, we use the SCS to study the effect of changes in lipid organization on the lipid barrier function using benzoic acid as permeation compound. First, in the SCS, we increased the level of one of the three major lipid classes keeping the ratio between the other lipid classes constant. An increased cholesterol level resulted in an increase in phase-separated cholesterol and a reduction in the permeability. An increase in ceramide or free fatty acid level resulted in the formation of additional phases, but had no significant influence on the permeability. We also examined models that mimic selected changes in lipid composition reported for dry or diseased skin. The SCS that mimics the composition in recessive X-linked ichthyosis skin displayed a two-fold increase in permeability. This increase is possibly related to the formation of an additional, less ordered phase in this model.

© 2011 Elsevier B.V. All rights reserved.

## 1. Introduction

The physical barrier of the human skin is located in the uppermost layer, the stratum corneum (SC). The SC consists of enucleated dead cells (corneocytes) that are surrounded by lipid lamellae. As these lipid lamellae form a continuous pathway in the SC, the lipid domains are considered to play a dominant role in the skin barrier function [1]. The main lipid classes in the SC are ceramides (CER), cholesterol (CHOL), and free fatty acids (FFA) [2–6]. The lipids are arranged in two crystalline coexisting lamellar phases with repeat distances of 13 and 6 nm, respectively. These lamellar phases are referred to as the long periodicity phase (LPP) and the short periodicity phase (SPP) [7,8]. At the skin temperature of 30–32 °C, in human SC, the lipids in the lipid lamellae are organized mainly in an orthorhombic lateral packing, although a subpopulation of lipids also forms a hexagonal or even a liquid-like lateral packing [9–11]. The lateral and lamellar lipid organization are considered to play an important role in the skin barrier function [11–13]. When focusing in more detail on the lipid composition, a wide distribution of FFA chain lengths has been identified. The most abundant chain lengths in the FFA mixture are those of 22 and 24 C atoms [14]. As far as the CER are concerned, currently, there are eleven subclasses of CER identified in human SC

[2,3,6]. To understand the change in lipid phase behavior in diseased and dry skin [15–19], we should unravel the complex phase behavior in SC. As it is impossible to perform these studies with intact SC, lipid mixtures should be used mimicking the lipid phase behavior of SC as closely as possible. In previous studies, lipid mixtures were prepared using isolated as well as synthetic CER mixtures. These lipid mixtures mimicked the lipid organization of SC very closely and provided useful information on the role the lipid classes play in the lipid phase behavior [20–22]. However, no information was obtained about the relation between lipid organization and the skin barrier function. In order to study this, we developed a skin lipid membrane consisting of a porous substrate covered with a mixture of synthetic CER, CHOL, and FFA. This membrane is referred to as the stratum corneum substitute (SCS). The SCS mimics the lipid organization and lipid orientation in SC very closely. As the lipid composition can easily be modified, the SCS allows us to study the relationship between lipid composition, molecular organization, and barrier function in just one model [23–25]. In a previous study, it was observed that the LPP plays an important role in the skin barrier function [23]. In a recent paper, we examined also the effect of the lateral packing on the permeability of the SCS using benzoic acid (BA), a medium lipophilic low molecular weight compound, as model drug [26]. This study revealed that an orthorhombic to hexagonal transition does not affect the diffusivity of BA in the SCS.

In the present study, we will first systematically change the CER, CHOL, and FFA composition. Subsequently, we examine models that mimic some aspects of the changes in lipid

\* Corresponding author. Leiden/Amsterdam Center for Drug Research, Department of Drug Delivery Technology, Gorlaeus Laboratories, University of Leiden, P.O. Box 9502, 2300 RA Leiden, The Netherlands. Tel.: +31 715274208.

E-mail address: [bouwstra@chem.leidenuniv.nl](mailto:bouwstra@chem.leidenuniv.nl) (J.A. Bouwstra).

composition reported for SC of dry skin (winter xerosis), recessive X-linked ichthyosis, and psoriasis skin. The permeability of the *in vitro* SCS models is assessed by measuring the permeation of BA. To examine the lipid organization in the models, Fourier transform infrared spectrometry (FTIR) and small-angle X-ray diffraction (SAXD) are used.

## 2. Materials and methods

### 2.1. Materials

Synthetic CER(EOS)C30-linoleate, CER(EOS)C30-oleate, CER(NS)C24, CER(NP)C24, CER(NP)C16, CER(AS)C24, and CER(AP)C24 (see Fig. 1) were generously provided by Cosmoferm B.V. (Delft, The Netherlands). Palmitic acid (C16:0), stearic acid (C18:0), arachidic acid (C20:0), behenic acid (C22:0), tricosanoic acid (C23:0), lignoceric acid (C24:0), cerotic acid (C26:0), and cholesterol were purchased from Sigma–Aldrich Chemie GmbH (Schnellendorf, Germany). Benzoic acid was obtained from Sigma–Aldrich (Zwijndrecht, The Netherlands). Nuclepore polycarbonate filter disks (pore size 50 nm) were purchased from Whatman (Kent, UK). All organic solvents are of analytical grade and manufactured by Labscan Ltd. (Dublin, Ireland). All other chemicals are of analytical grade and the water is of Millipore quality.

### 2.2. Preparation of the model lipid mixtures

For the preparation of the SCS models, CHOL, synthetic CER, and FFA were used in the appropriate molar ratio according to the different models. In Table 1, the ratios of the main lipid classes are displayed for the models used in this study. The main CER subclasses we have available consist of either a sphingosine (S) or phytosphingosine (P) base, whereas the acyl chain is a nonhydroxy (N),  $\alpha$ -hydroxy (A), or  $\omega$ -hydroxy chain [27]. The corresponding nonhydroxy and  $\alpha$ -hydroxy CER that are used in

this study are denoted as CER NP, CER NS, CER AP, and CER AS. The  $\omega$ -hydroxy CER possesses a longer acyl chain length (C30) and has a linoleic or oleic acid ester-linked to their  $\omega$ -hydroxy group (indicated with EO). In our study, we use two such acylCERs, denoted as CER(EOS)-linoleate and CER(EOS)-oleate. For the ceramides mixture (CER), the following synthCER composition was selected (see Fig. 1): CER(EOS)C30-linoleate, CER(NS)C24, CER(NP)C24, CER(AS)C24, CER(NP)C16, and CER(AP)C24 in a 15:51:16:4:9:5 M ratio, similar as observed in pig SC [22]. The acyl chain length of the various CER subclasses is either 30 C atoms (C30), 24 C atoms (C24), or 16 C atoms (C16). For the free fatty acids mixture (FFA), the following composition was selected: C16:0, C18:0, C20:0, C22:0, C23:0, C24:0, and C26:0 at a molar ratio of 1.8:4.0:7.7:42.6:5.2:34.7:4.1, respectively. This chain length distribution is based on the reported FFA composition in SC [14]. For each model, the appropriate amounts of individual lipids were dissolved in chloroform:methanol (2:1 v/v). After evaporation of the organic solvent under a stream of nitrogen, the lipid mixtures were re-dissolved either in hexane:ethanol 2:1 v/v (for models used in permeability and X-ray studies) or in chloroform:methanol 2:1 v/v (for models used in FTIR studies) at a total lipid concentration of 4.5 mg/ml.

### 2.3. Preparation of SCS models for *in vitro* permeability studies

A Linomat IV (Camag, Muttenz, Switzerland) extended with a y-axis arm was used to spray lipids in hexane:ethanol solution from a distance of 1 mm onto a porous filter substrate. The spraying flow rate was 5.0  $\mu$ l/min at a movement speed of 1.0 cm/s. In an area of  $8 \times 8$  mm<sup>2</sup>, 0.90 mg of lipids was applied per SCS model. After spraying, the SCS was equilibrated at around 80 °C. After an equilibration period of at least 10 min, the SCS was cooled down to room temperature in approximately 30 min.

### 2.4. Preparation of lipid models for FTIR studies

Sample preparation for FTIR was the same as above, but instead 1.5 mg of lipids in a chloroform:methanol solution was sprayed in an area of  $1 \times 1$  cm<sup>2</sup> on an AgBr window. The sample was equilibrated for 10 min at around 80 °C and slowly cooled down to room temperature in about 30 min. Subsequently, the lipid layer was covered with 25  $\mu$ l of deuterated acetate buffer pH 5 (50 mM) and stored at 37 °C for 24 h to fully hydrate the sample. Finally, to homogenize the sample, five freeze-thawing cycles of 3 h each were carried out between –20 °C and RT [28].

### 2.5. Permeability studies

*In vitro* permeation studies were performed using Permeagear inline diffusion cells (Bethlehem PA, USA) with a diffusion area of 0.28 cm<sup>2</sup>. The SCS models were mounted in the diffusion cells and were hydrated for 1 h in phosphate-buffered saline (PBS: NaCl, Na<sub>2</sub>HPO<sub>4</sub>, KH<sub>2</sub>PO<sub>4</sub>, and KCl in MQ water with a concentration of 8.13, 1.14, 0.20, and 0.19 g/l, respectively) at pH 7.4 prior to the experiment. The donor compartment was filled with 1.4 ml of BA (MW 122 g/mol) solution in PBS (pH 7.4) at a 2.0 mg/ml concentration. BA has a log  $P_{\text{oct/water}}$  value of about 1.7. The acceptor phase consisted of PBS (pH 7.4), which was perfused at a flow rate of about 2 ml/h. The acceptor phase was stirred with a magnetic stirrer. The volume per collected fraction was determined by weighing. Each experiment was performed under occlusive conditions, by closing the opening of the donor compartment with adhesive tape. To mimic the *in vivo* conditions as close as possible, the temperature of the SCS was maintained at 32 °C during the permeation studies, using a thermo-stated water bath.

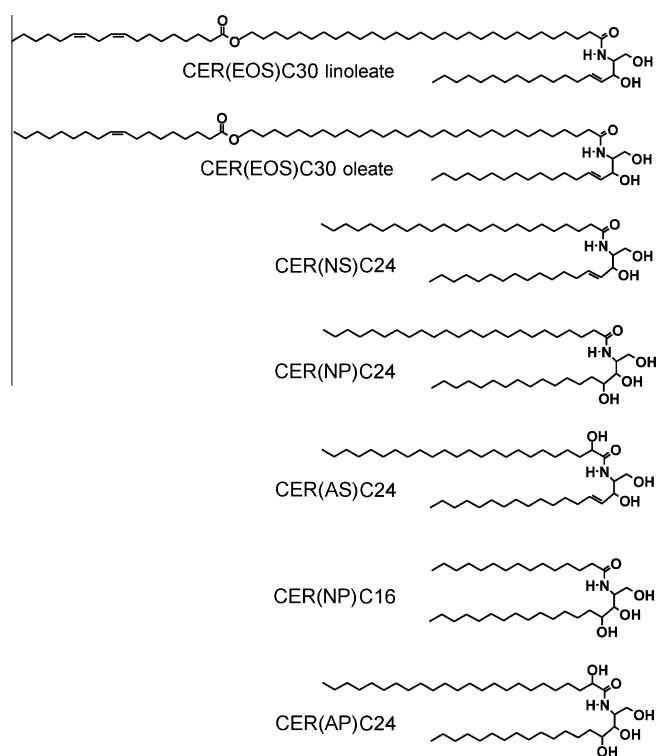


**Fig. 1.** Molecular structure of the synthetic CER selected for the lipid mixtures (see Table 1). The nomenclature is according to Motta et al. [27].

**Table 1**

Results of the permeation studies with benzoic acid using the various membranes.

Model type	Abbreviation	Composition and molar ratio		$J_{ss}$ ( $\mu\text{g}/\text{cm}^2/\text{h}$ )	$\tau$ (h)
SC substitute	SCS	CER:CHOL:FFA	1:1:1	$24 \pm 2^b$	$1.1 \pm 0.5^b$
High CER level		CER:CHOL:FFA	2:1:1	$22.5 \pm 1.8$	$-0.3 \pm 0.5$
High CHOL level		CER:CHOL:FFA	1:2:1	$9.0 \pm 1.5$	$0.6 \pm 0.6$
High FFA level		CER:CHOL:FFA	1:1:2	$25.6 \pm 1.2^c$	n.a.
Psoriasis model	PS SCS	CER:CHOL:FFA	1:1.2:0.5	$14.5 \pm 1.1$	$0.3 \pm 0.2$
Winter xerosis model	WX SCS	CER <sup>a</sup> :CHOL:FFA	1:1:1	$15.6 \pm 2.6$	$0.9 \pm 0.8$
Recessive X-linked ichthyosis	RXLI SCS	CER:CHOL:FFA:ChSO <sub>4</sub>	1:1:1:0.33	$46.2 \pm 5.5$	$0.1 \pm 0.3$

<sup>a</sup> In the CER composition of the winter xerosis model, 50% of the CER(EOS)-linoleate is replaced by CER(EOS)-oleate.<sup>b</sup> For the equimolar SCS,  $J_{ss}$  and  $\tau$  were obtained in a previous study [25].<sup>c</sup> For the SCS with a high FFA level,  $J_{ss}$  was determined from the last 4 flux values, therefore,  $\tau$  could not be calculated.

Steady-state fluxes and lag-times were determined from a plot of the cumulative permeated amount. The steady-state flux ( $J_{ss}$ ) is the slope of the linear part of this graph and the lag-time ( $\tau$ ) is determined by regression of this linear part to the time when the permeated amount is 0.

## 2.6. FTIR studies

All spectra were acquired on a BIORAD FTS4000 FTIR spectrometer (Cambridge, Massachusetts) equipped with a broad-band mercury cadmium telluride detector, cooled with liquid nitrogen. The sample cell was closed by two AgBr windows. The sample was under continuous dry air purge starting 1 h before the data acquisition. The spectra were collected in transmission mode, as a co-addition of 256 scans at  $1 \text{ cm}^{-1}$  resolution during 4 min. In order to detect the phase transitions, the sample temperature was increased at a heating rate of  $0.25 \text{ }^\circ\text{C}/\text{min}$ , resulting in a  $1 \text{ }^\circ\text{C}$  temperature rise per recorded spectrum. The spectra were collected between  $0 \text{ }^\circ\text{C}$  and  $90 \text{ }^\circ\text{C}$ . The software used was Win-IR pro 3.0 from Biorad (Cambridge, Massachusetts). The spectra were deconvoluted using a half-width of  $5 \text{ cm}^{-1}$  and an enhancement factor of 2.0.

## 2.7. Determining the midpoint temperature of the melting transition and fitting of the rocking vibrations in FTIR

In FTIR, the frequency of the symmetric stretching maximum as function of temperature depicts the transition of the lipids to a liquid phase [29,30]. The midpoint temperature ( $T_m$ ) of the melting transition was determined as the temperature at which the frequency increase is halfway between two fitted straight parts of the curve before and after the transition. The straight parts before and after the transition are fitted by linear fits and the data point closest to the transition that deviates from the linear fit is chosen as the beginning or end point of the melting transition. This method for determining  $T_m$  is depicted in Fig. 2B-ii.

The frequency of the two rocking maxima as function of temperature depicts the phase transition from an orthorhombic to a hexagonal lateral packing [31,32]. During this transition, at those temperatures at which no separate peaks could be distinguished but only an asymmetric peak, two components were fitted to the rocking vibrations in order to determine the position of the high-frequency component. The curve-fitting procedure was as follows: First, in the range from  $635$  to  $900 \text{ cm}^{-1}$  in the FTIR spectrum, a baseline was created with a constant value corresponding to the lowest value in that part of the spectrum. Subsequently, the two components present in the spectrum were fitted with two Lorentzian peak shapes using a least squares approximation. The position of the maximum of the high-frequency component was subsequently used in the plot of the rocking frequencies as function of temperature. In this plot, the positions of the high-frequency

component are displayed until a temperature is reached at which the high-frequency component could no longer be fitted.

## 2.8. SAXD studies

X-ray diffraction was used to obtain information about the lamellar organization (i.e., the repeat distance of a lamellar phase) and the orientation of the lamellae. The SCS was mounted parallel to the primary beam in a temperature-controlled sample holder with mica windows. Static diffraction patterns were collected for 1 min at  $25 \text{ }^\circ\text{C}$ . The scattering intensity  $I$  (in arbitrary units) was measured as a function of the scattering vector  $q$  (in reciprocal nm). The latter is defined as  $q = (4\pi \sin \theta) / \lambda$ , in which  $\theta$  is the scattering angle and  $\lambda$  is the wavelength. From the positions of a series of equidistant peaks ( $q_n$ ), the periodicity, or  $d$ -spacing, of a lamellar phase was calculated using the equation  $q_n = 2n\pi/d$ , with  $n$  being the order number of the diffraction peak. One-dimensional intensity profiles were obtained by transformation of the two-dimensional SAXD detector pattern from Cartesian ( $x, y$ ) to polar ( $\rho, \theta$ ) coordinates and subsequently integrating over  $\theta$ . All measurements were performed at the European Synchrotron Radiation Facility (ESRF, Grenoble) using station BM26B. The X-ray wavelength and the sample-to-detector distance were  $0.113 \text{ nm}$  and  $0.419 \text{ m}$ , respectively. Diffraction data were collected on a Frelon 2000 CCD detector with  $2048 \times 2048$  pixels at  $14 \text{ }\mu\text{m}$  spatial resolution and  $5\times$  magnification. The spatial calibration of this detector was performed using silver behenate ( $d = 5.838 \text{ nm}$ ) and the two strongest reflections of high density polyethylene (HDPE,  $d = 0.4166$  and  $0.378 \text{ nm}$ ).

## 3. Results

To assess the barrier properties of the various SCS models, the permeation of the model compound BA has been measured at the skin temperature of about  $32 \text{ }^\circ\text{C}$ . To correlate permeability with lipid organization, the lipid organization has been examined with FTIR and SAXD. The various model compositions, steady-state flux values, and lag-times are presented in Table 1.

### 3.1. Influence of the CER:CHOL:FFA ratio on the barrier function of SCS

To determine the role of each of the lipid classes on the lipid composition and permeability, SCS varying systematically in CER:CHOL:FFA composition were examined. The fluxes are provided in Table 1. In this table, the flux across SCS with an equimolar CER:CHOL:FFA composition that was reported previously [25] is also provided. In Fig. 2A-i, the BA flux profile across the SCS with a CER:CHOL:FFA molar ratio of 2:1:1 is shown. The steady-state flux is  $22.5 \pm 1.8 \text{ }\mu\text{g}/\text{cm}^2/\text{h}$  and the lag-time is  $-0.3 \pm 0.5 \text{ h}$ .

The  $\text{CH}_2$  symmetric stretching frequencies in the infrared spectrum provide information about the conformational ordering of the

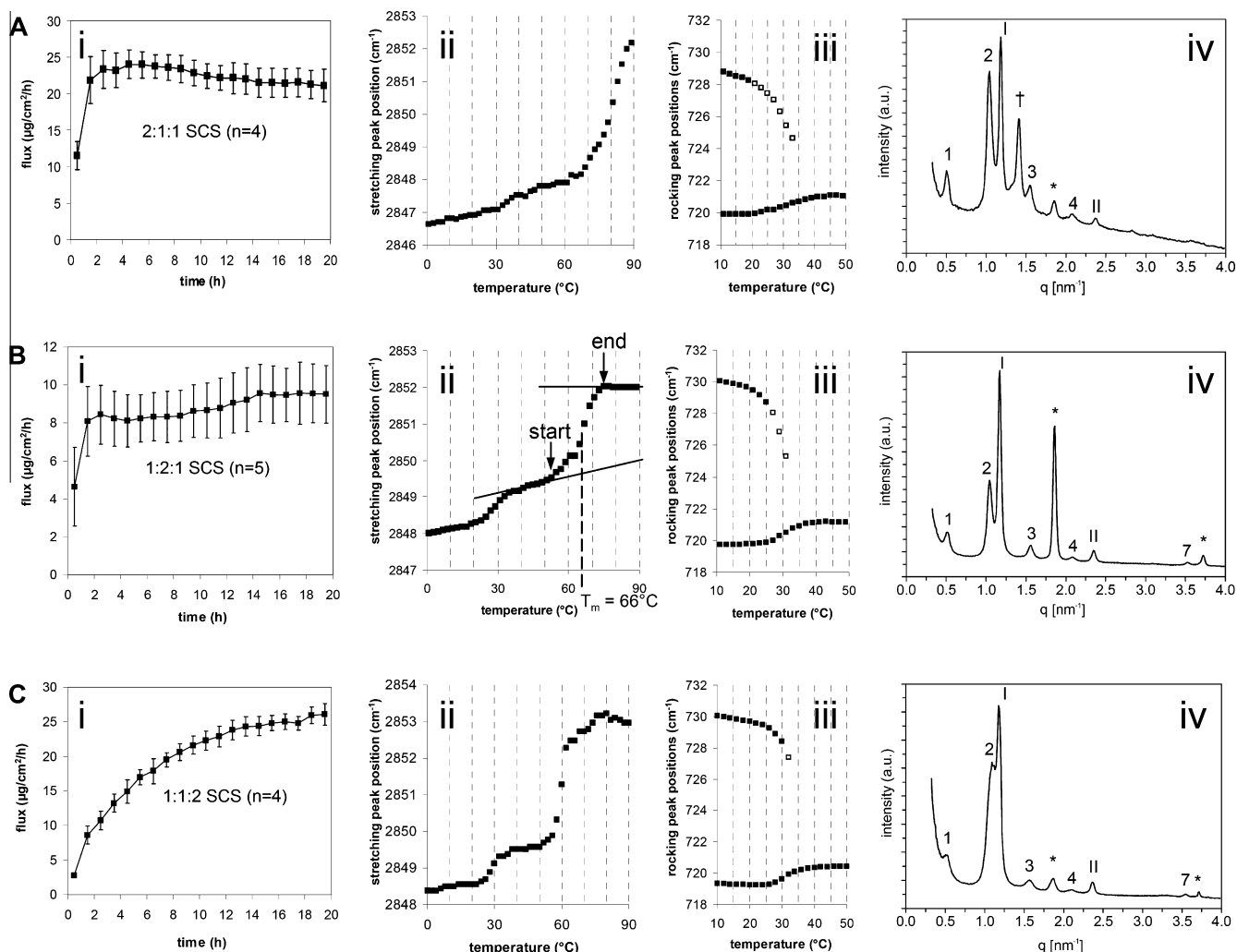


**Fig. 2.** (i) Plots of the BA permeation versus time, (ii)  $\text{CH}_2$  symmetric stretching frequency as function of temperature, (iii) thermotropic response of the FTIR  $\text{CH}_2$  rocking frequencies, and (iv) the SAXD pattern of (A) SCS in 2:1:1 CER:CHOL:FFA molar ratio, (B) SCS in a 1:2:1 CER:CHOL:FFA molar ratio (C) SCS in a 1:2:1 CER:CHOL:FFA molar ratio. In the SAXD patterns, the Arabic numbers denote diffraction orders of the LPP, the Roman numbers indicate reflections assigned to the SPP, and asterisks mark the reflections of crystalline CHOL. The reflection that was assigned to an additional lamellar phase is indicated by a cross. In the figures depicting the  $\text{CH}_2$  rocking vibrations, the open squares are calculated with the peak fitting procedure.

lipid tails. The position of the  $\text{CH}_2$  symmetric stretching vibration as function of temperature is plotted in Fig. 2A-ii. At 20 °C, this frequency is  $2846.9\text{ cm}^{-1}$ , indicating a high conformational ordering. When increasing the temperature, between 30 and 40 °C, a weak shift is observed in frequency from  $2847.1$  to  $2847.5\text{ cm}^{-1}$ . Although not very pronounced, it indicates an orthorhombic to hexagonal transition. Increasing the temperature leads to another shift in frequency from  $2848.1$  to  $2852.2\text{ cm}^{-1}$  between 65 and 89 °C, revealing the transition to a liquid phase, with a midpoint temperature of  $T_m = 80\text{ °C}$ .

The FTIR rocking frequencies provide detailed information on the lateral packing. Due to short range coupling, the orthorhombic packing is characterized by a doublet at approximately 720 and  $730\text{ cm}^{-1}$ , while the hexagonal packing is characterized by a singlet at a vibration frequency of approximately  $720\text{ cm}^{-1}$ . The thermotropic response of the rocking frequencies in Fig. 2A-iii shows a shift of the high-frequency component from  $728.0$  to  $724.6\text{ cm}^{-1}$  between 21 and 33 °C, suggesting the transition from an orthorhombic to a hexagonal lateral packing in this temperature region.

The SAXD pattern of the 2:1:1 SCS in Fig. 2A-iv displays four diffraction peaks that can be ascribed to a LPP with a periodicity of

$12.0\text{ nm}$  and two reflections attributed to a SPP with periodicity of  $5.3\text{ nm}$ . Furthermore, an additional diffraction peak is observed indicative for an additional phase with a periodicity of  $4.4\text{ nm}$ , most likely due to phase-separated CER-rich domains. The peak at  $q = 1.85\text{ nm}^{-1}$  indicates the presence of a low level of phase-separated crystalline CHOL.

The SCS with elevated CHOL level was also studied. The permeability of the SCS with a CER:CHOL:FFA composition of 1:2:1 is displayed in Fig. 2B-i. This figure demonstrates that by increasing the CHOL levels, the BA flux drastically reduces since the steady-state flux is only  $9.0 \pm 1.5\text{ µg/cm}^2/\text{h}$ . The lag-time of this membrane is  $0.6 \pm 0.6\text{ h}$ .

The thermotropic response of the  $\text{CH}_2$  stretching frequencies is provided in Fig. 2B-ii. There is a gradual increase in the frequencies from 0 to 20 °C. At 20 °C, the symmetric stretching frequency is  $2848.3\text{ cm}^{-1}$ , denoting the presence of conformational ordered phases. A further increase in temperature from 21 to 37 °C results in a shift in frequency from  $2848.3$  to  $2849.1\text{ cm}^{-1}$ , indicative for the orthorhombic-hexagonal phase transition. Upon further heating between 50 and 79 °C, a second transition is observed from  $2849.4$  to  $2852.0\text{ cm}^{-1}$ , demonstrating the formation of a liquid phase. The midpoint temperature of this transition is  $66\text{ °C}$ .

The rocking frequencies are displayed in Fig. 2B-iii. The orthorhombic to hexagonal transition is shown by a shift of the high-frequency component from 729.5 to 725.3  $\text{cm}^{-1}$  between 21 and 31 °C.

The SAXD pattern of the 1:2:1 SCS is displayed in Fig. 2B-iv with diffraction peaks attributed to the LPP and SPP. However, the diffraction peaks attributed to crystalline CHOL have a high intensity, demonstrating a high level of phase-separated CHOL.

The level of the third main class of lipids is also increased in the SCS. In Fig. 2C-i, the permeability curve of SCS with a CER:CHOL:FA molar ratio of 1:1:2 is displayed. From this figure, it is clear that a steady-state flux is not reached within the 20 h of permeation. The flux value was calculated as a mean of the flux values between 16 and 20 h of permeation and is  $25.6 \pm 1.2 \mu\text{g}/\text{cm}^2/\text{h}$ . The lag-time could not be determined due to the absence of a steady-state flux.

The thermotropic  $\text{CH}_2$  stretching response is provided in Fig. 2C-ii. At low temperatures, the lipid tails are in a conformational ordering as shown by the  $\text{CH}_2$  stretching frequency of 2848.6  $\text{cm}^{-1}$  at 20 °C. Upon increasing the temperature, a clear shift in frequency from 2848.6 to 2849.5  $\text{cm}^{-1}$  is observed between 22 and 38 °C, demonstrating the orthorhombic to hexagonal phase transition. When further increasing the temperature, another shift in wavenumber from 2849.6 to 2852.8  $\text{cm}^{-1}$  is visible between 50 and 72 °C denoting the transition to a liquid phase with a midpoint temperature of 60 °C.

The orthorhombic to hexagonal phase transition is also monitored by the thermotropic  $\text{CH}_2$  rocking response as displayed in Fig. 2C-iii: A shift of the high-frequency component from 729.5 to 727.4  $\text{cm}^{-1}$  is observed between 24 and 32 °C. When increasing the temperature further, a weak orthorhombic component remained in the rocking curve until a temperature of 60 °C. This indicates that the majority of the lipids form a hexagonal lateral packing around 34 °C, but a small fraction of phase-separated FFA remains in the orthorhombic packing until a temperature of about 60 °C is reached [28]. At this temperature, the crystalline FFA starts to transform into a liquid phase.

The SAXD pattern of the model with high FFA level is displayed in Fig. 2C-iv. It depicts two diffraction peaks attributed to the SPP with a periodicity of 5.3 nm. Five diffraction peaks could be identified that are attributed to the LPP with a periodicity of 12.0 nm. The two peaks at  $q = 1.85$  and  $3.7 \text{ nm}^{-1}$  indicate the presence of a low level of phase-separated crystalline CHOL. The elevated FFA level did not result in an additional phase with a long range ordering.

### 3.2. The permeability and phase behavior of SCS with a lipid composition based on that in dry or diseased skin

The lipid organization and barrier properties of models with compositions related to dry skin (winter xerosis), recessive X-linked ichthyosis, and psoriasis skin were also examined.

Due to seasonal influences, the lipid composition in the SC is reported to undergo changes. Focussing on the CER subclasses, in the winter season, the relative level of CER(EOS)-oleate is increased at the expense of CER(EOS)-linoleate [18,33]. To mimic this aspect of the SC composition of dry skin (winter xerosis), 50% of the CER(EOS)-linoleate was replaced by CER(EOS)-oleate in the SCS. The SCS that mimics the composition in SC of dry skin is referred to as WX SCS. The permeation curve of BA through WX SCS is displayed in Fig. 3A-i. The steady-state flux is  $15.6 \pm 2.6 \mu\text{g}/\text{cm}^2/\text{h}$  and the lag-time  $0.9 \pm 0.8 \text{ h}$ .

The thermotropic response of the  $\text{CH}_2$  symmetric stretching peak is plotted in Fig. 3A-ii. At low temperatures, a gradual increase in frequency is observed up to 2848.7  $\text{cm}^{-1}$  at 20 °C. Upon increasing the temperature from 21 to 41 °C, a shift in wavenumber from 2848.8 to 2849.9  $\text{cm}^{-1}$  is detected, indicating the orthorhombic to hexagonal phase transition. When further increasing

the temperature, a liquid phase is formed between 51 and 73 °C as denoted by a shift from 2850.1 to 2853.2  $\text{cm}^{-1}$ . The midpoint temperature of this transition is 60 °C.

The FTIR rocking frequencies displayed in Fig. 3A-iii show a shift of the high-frequency component from 729.1 to 724.4  $\text{cm}^{-1}$  between 25 and 33 °C, characteristic for the orthorhombic-hexagonal transition.

The SAXD pattern of WX SCS is shown in Fig. 3A-iv. It displays two diffraction peaks attributed to a SPP with a periodicity of 5.3 nm and five diffraction peaks assigned to the LPP with a periodicity of 12.0 nm. Crystalline CHOL is also present, as indicated by two diffraction peaks at  $q = 1.85$  and  $3.7 \text{ nm}^{-1}$ .

Besides a change in CER:CHOL:FA molar ratio, a difference in the CER composition of psoriatic scale, compared to normal human stratum corneum, is reported in literature [17,27]. However, in our present studies, we will only focus on the change in CER:CHOL:FA molar ratio on the permeability, to establish whether this change can account for an increased permeability in psoriasis skin. Based on the results of Motta et al., the CER:CHOL:FA molar ratio in the SCS model was adapted to 1.0:1.2:0.5 [17]. This model is referred to as PS SCS. The flux profile of PS SCS is displayed in Fig. 3B-i, displaying a steady-state flux of  $14.5 \pm 1.1 \mu\text{g}/\text{cm}^2/\text{h}$  and a lag-time of  $0.3 \pm 0.2 \text{ h}$ .

The thermotropic response of the  $\text{CH}_2$  stretching vibrations is displayed in Fig. 3B-ii. The maximum of the symmetric stretching frequencies at 20 °C is 2847.5  $\text{cm}^{-1}$ . Upon increasing the temperature, a small shift in peak position is visible around 30 °C, possibly revealing the orthorhombic to hexagonal transition. Upon further heating, a shift in wavenumber is visible between 50 and 80 °C, indicative for the transition to a liquid phase. This transition has a  $T_m$  of 72 °C.

The FTIR rocking frequencies in Fig. 3B-iii show a gradual shift of the high-frequency component from 728.2 to 724.8  $\text{cm}^{-1}$  between 25 and 33 °C, indicating the transition from orthorhombic to hexagonal lateral packing.

The SAXD pattern of PS SCS is depicted in Fig. 3B-iv. It displays two diffraction orders associated to a SPP, with a periodicity of 5.2 nm. Also, four diffraction peaks assigned to a LPP with a periodicity of 12.0 nm are observed. A high amount of CHOL is phase separated as reflected by the high intensity of the diffraction peaks attributed to crystalline CHOL.

The pathological scaling in recessive X-linked ichthyosis skin is associated with accumulation of abnormally high quantities of  $\text{ChSO}_4$  in the SC [15,16,19]. On this basis, we prepared a model for the lipid composition by addition of  $\text{ChSO}_4$  at a molar ratio of 0.33. This model is referred to as RXLI SCS. The permeation curve of BA through RXLI SCS is displayed in Fig. 3C-i, showing a high steady-state flux of  $46.2 \pm 5.5 \mu\text{g}/\text{cm}^2/\text{h}$  and a short lag-time of  $0.1 \pm 0.3 \text{ h}$ .

The FTIR stretching maxima in Fig. 3C-ii display a constant value of 2848.6  $\text{cm}^{-1}$  from 0 to 20 °C, indicating conformational ordering of the lipid tails. Upon increasing the temperature, a first shift from 2848.6 to 2849.6  $\text{cm}^{-1}$  is observed between 20 and 40 °C, representative for an orthorhombic to hexagonal transition. Further increasing the temperature leads to a second shift in wavenumber from 2849.9 to 2852.4  $\text{cm}^{-1}$  between 59 and 77 °C, representing the transition to a fluid phase with a midpoint temperature of 68 °C.

The FTIR rocking frequencies of RXLI SCS in Fig. 3C-iii reveal a change from orthorhombic to hexagonal transition as shown by a change in high-frequency component from 729.0 to 724.0  $\text{cm}^{-1}$  between 25 and 31 °C.

The SAXD pattern of RXLI SCS is displayed in Fig. 3C-iv. It displays two diffraction peaks attributed to a SPP with a periodicity of 5.3 nm. The first-order reflection of the SPP is broad and contains a shoulder at approximately  $q = 1.4 \text{ nm}^{-1}$  which could indicate the

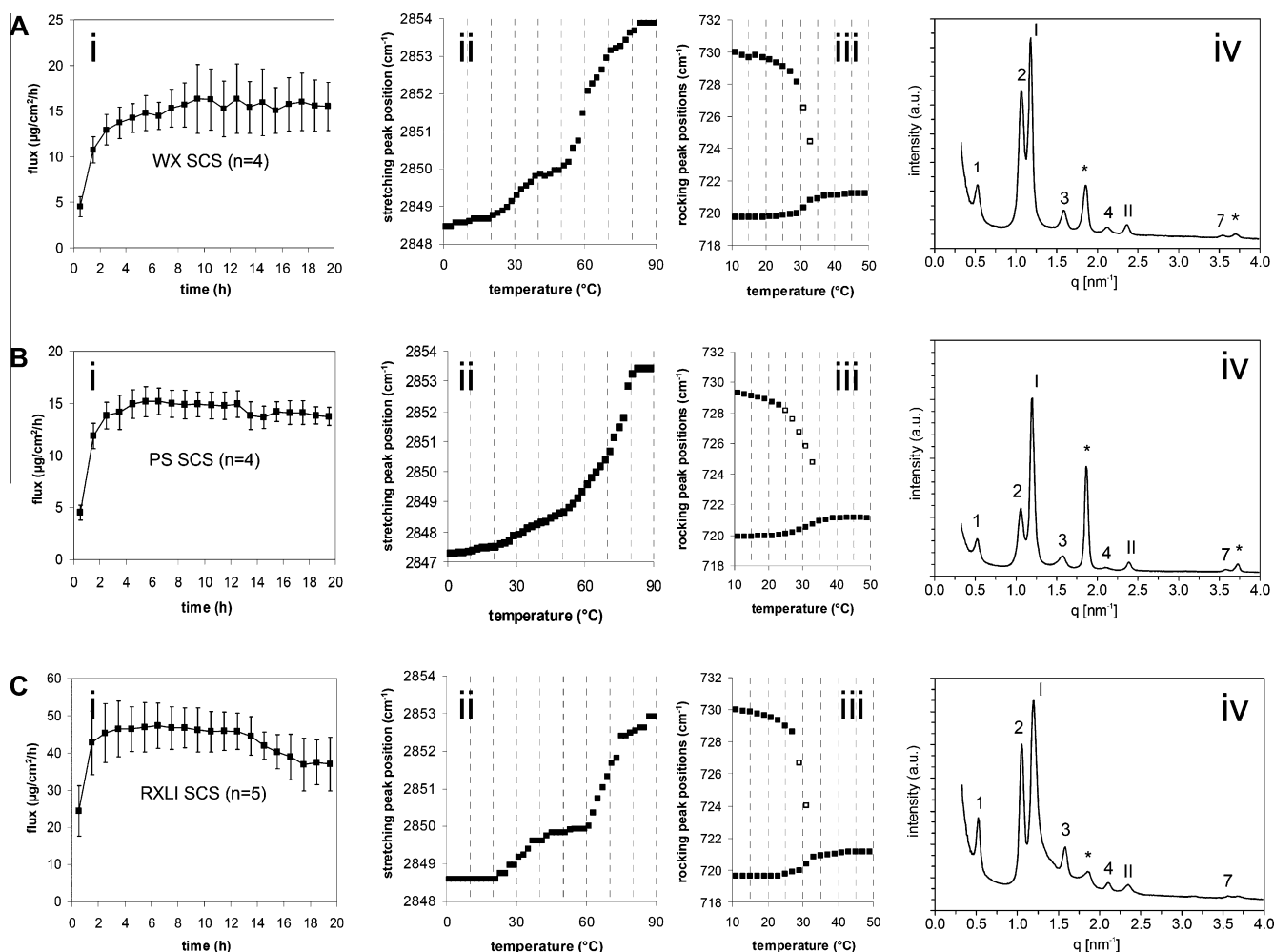


**Fig. 3.** (i) Plots of the BA permeation versus time, (ii)  $\text{CH}_2$  symmetric stretching frequency as function of temperature, (iii) thermotropic response of the FTIR  $\text{CH}_2$  rocking frequencies, and (iv) the SAXD pattern of (A) WX SCS, (B) PS SCS, and (C) RXLI SCS. In the SAXD patterns, the Arabic numbers denote diffraction orders of the LPP, the Roman numbers indicate reflections assigned to the SPP, and asterisks mark the reflections of crystalline CHOL. In the figures depicting the  $\text{CH}_2$  rocking vibrations, the open squares are calculated with the peak fitting procedure.

formation of an additional phase. Furthermore, five diffraction peaks are observed assigned to the LPP with a periodicity of 12.0 nm. The two diffraction peaks that are associated to crystalline CHOL are low in intensity, indicating a low level of phase-separated CHOL.

#### 4. Discussion

In the studies described in this paper, we focused on a systematic change in lipid composition to relate lipid composition and organization with permeability. For this purpose, we utilized a SC model membrane to unravel the role the various lipid classes play in the skin barrier function. In addition, we focused on the lipid permeability in diseased and dry skin. For this purpose, we constructed models for the SC lipid composition reported in winter xerosis, psoriasis, and recessive X-linked ichthyosis skin. To study the permeability of the various models, we used BA as a model drug.

##### 4.1. The order–disorder transition temperature is related to the symmetric $\text{CH}_2$ stretching vibrations of the lipid tails at 20 $^{\circ}\text{C}$

When closely examining the FTIR data of all models, it is observed that the models with a high conformational order at room

temperature (i.e., low wavenumber of the  $\text{CH}_2$  symmetric stretching peak position at 20  $^{\circ}\text{C}$ ) exhibit a relatively high melting transition midpoint temperature. To gain more insight into this relationship, we plotted the  $\text{CH}_2$  symmetric stretching vibration at 20  $^{\circ}\text{C}$  against the midpoint temperature of the melting transition in each model, see Fig. 4. Although the midpoint temperature of the melting transition has no physical meaning, as the symmetric stretching peak in FTIR is composed of several vibrational components, it enables us to determine whether this phase transition is related to the conformational order of the lipid chains at 20  $^{\circ}\text{C}$ . We also included data of the equimolar SCS and a model with short chain FFA, examined in a previous study [26]. As depicted in Fig. 4, a linear correlation is observed: the symmetric stretching wavenumber (chain conformation) at 20  $^{\circ}\text{C}$  decreases linearly with increasing melting transition  $T_m$ .

From this graph, it is clear that when using the same ceramide composition, an increase in conformational ordering results in an increase in the melting transition  $T_m$ . When focusing on those samples in which the FFA content varied, the results are quite remarkable. Although the FFA induces the formation of an orthorhombic lateral packing, it also induces a reduction in the ordering of the chains and a reduction in the  $T_m$ . This might be due to the change in headgroup interactions, as it has been suggested (based on pure ceramides but also on mixtures) that an increase in hydrogen bond

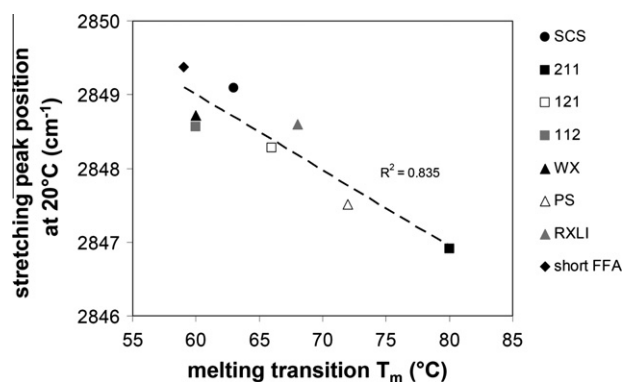


Fig. 4. The midpoint temperature of the melting transition as function of the conformational order at 20 °C. Depicted are data of all models used in this study plus data of equimolar SCS and of a model with short chain FFA, examined in a previous study [26].

density in the headgroup region increases the conformational ordering and raises the  $T_m$  of the order–disorder transition [34,35]. This suggests that the addition of FFA increases the packing density but reduces the number of hydrogen bonds.

#### 4.2. Deviation from the equimolar CER:CHOL:FFA ratio observed in human SC does not always result in a decreased barrier function

As it has been suggested that the lipid composition and organization play an important role in the skin barrier, in this study, we examined the effect of the lipid composition and organization of the SCS on its permeability. In previous studies, we reported the permeability and lipid phase behavior of the equimolar CER:CHOL:FFA SCS, mimicking the lipid composition and skin barrier of healthy subjects [25,26]. The BA steady-state flux across this SCS was  $24 \pm 2 \mu\text{g}/\text{cm}^2/\text{h}$  and the lag-time was  $1.1 \pm 0.5 \text{ h}$  [25]. From the FTIR data presented in a recent study [26], the midpoint temperature of the transition from a hexagonal to a liquid phase was 63 °C and the orthorhombic-hexagonal transition occurred between 20 and 36 °C. In the same study, we observed that the flux of BA was more sensitive for a change in the lamellar phases than for a phase change from an orthorhombic to a hexagonal packing. In the present study, we varied the lipid composition by increasing the level of either CER, CHOL, or FFA. The formation of a hexagonal phase in these studies is not determinative for the changes in flux.

When increasing the level of CER or CHOL by a factor two compared to the equimolar ratio, the X-ray diffraction curves clearly revealed phase separation. In the SCS with 2:1:1 CER:CHOL:FFA, an additional 4.4 nm phase was detected, while the CER:CHOL:FFA 1:2:1 SCS resulted in an enhanced level of phase-separated crystalline CHOL. The additional 4.4 nm phase did not affect the permeability, while the higher level of phase-separated CHOL in the SCS led to a twofold reduction in the permeability. The CHOL domains consist of densely packed three-dimensional crystals resulting in many spots and reflections in the WAXD pattern (not shown). If these three-dimensional crystals are not very permeable to BA, it will result in a reduction of the effective diffusion area of the SCS and in an increase in the permeation pathway. This will lead to a reduction in the steady-state flux. As far as the 4.4 nm phase is concerned, our results indicate that this phase has a similar layered structure as the SPP as no features in the diffraction pattern are observed indicating the presence of a three-dimensional crystalline structure (wide-angle X-ray data, unpublished results). This may explain why no change in permeability is observed in the presence of the 4.4 nm phase.

When comparing with the *in vivo* situation, the 4.4 nm phase was never observed in diffraction patterns of isolated human SC.

However, the presence of crystalline CHOL is frequently observed in human SC [8,36]. Therefore, the observation that an increase in phase-separated crystalline CHOL results in an increase in the skin barrier function is relevant for the *in vivo* situation.

In the 1:1:2 CER:CHOL:FFA SCS, no phase separation of FFA is observed when focusing on the long-range ordering (lamellar phases). However, the presence of a small shoulder was noticed in the high-frequency component of the FTIR rocking vibrations. This shoulder was present up to about 60 °C and indicates that a low level of FFA forms separate domains within the lipid lamellae. The flux of BA across the 1:1:2 CER:CHOL:FFA SCS displays a very long lag-time. As we used a PBS buffer of pH 7.4 in the donor and acceptor phase and the  $pK_a$  of FFA in ceramide containing mixtures is around 6.3 [37], the increase in lag-time may occur by an ionization of the FFA, which may be more pronounced at a high level of FFA, or in phase-separated FFA domains within the lipid lamellae.

As far as the diseased skin models are concerned, in these studies, we are limited by the information available in literature. Although changes in the composition of the lipid classes have been reported for cosmetically dry skin and for psoriasis, no information is available on the FFA and CER chain length distribution compared to that in skin of healthy subjects. A reduction in chain length of the CER and FFA may have a profound effect on the lipid organization and permeability. For this reason, our studies only provide information on the changes in permeability caused by the reported changes in the composition of the main lipid classes in the various skin diseases.

For both the WX SCS and PS SCS, the steady-state flux and lag-time are similar to that in the equimolar CER:CHOL:FFA SCS. The lamellar lipid organization of these models is also similar to that in the equimolar SCS and as the lamellar organization is a crucial factor in the skin permeability [11,26], it is not surprising that the WX SCS and PS SCS have a barrier function that is similar to the equimolar SCS. Although winter xerosis skin is known to be susceptible and displays a faulty desquamation [38,39] and psoriasis skin is characterized by a deranged keratinization process and an impaired barrier function [40], our results with BA as permeant demonstrate that the reported changes in CER(EOS)-oleate/linoleate ratio in dry skin or in CER:CHOL:FFA ratio in psoriasis skin may not be responsible for the observed impaired barrier function *in vivo*.

In contrast to the WX and PS models, the permeability of the RXLI model is about twice that of equimolar SCS. Therefore, the enhanced permeability indicates that the increased  $\text{ChSO}_4$  is expected to be at least partly responsible for the abnormal barrier function observed in RXLI skin [19]. The reduced barrier function in our lipid model may partly be explained by the lower level of phase-separated crystalline CHOL. The excess  $\text{ChSO}_4$  present in this model reduces the amount of crystalline CHOL, similarly as previously observed in a lipid model with isolated CER [41]. However, the reduced crystalline CHOL cannot explain the twofold increase in flux as the level of phase-separated crystalline CHOL in the 2:1:1 and 1:1:2 CER:CHOL:FFA SCS was also lower, while no increase in permeability was observed. Therefore, other factors should play a role. Previously, it was observed that  $\text{ChSO}_4$  induces a fluid phase in mixtures with isolated CER, CHOL, and FFA [42]. Such a fluid phase is expected to increase the permeability. However, at room temperature (20 °C), the frequency of  $\text{CH}_2$  symmetric stretching vibrations of the RXLI model was not shifted to a higher wavenumber as compared to equimolar SCS, indicating that the formation of a substantial level of fluid phase in SCS was not induced by the addition of  $\text{ChSO}_4$ . Perhaps the use of synthetic CER instead of isolated CER precludes the formation of a fluid phase in the RXLI SCS. In order to explain the increased permeability, we investigated the two-dimensional SAXD patterns in more detail

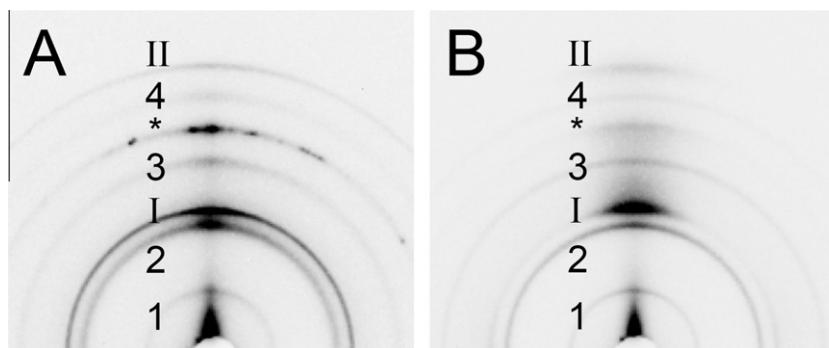


**Fig. 5.** Two-dimensional SAXD images. The Arabic numbers 1–4 denote diffraction orders of the LPP, the reflections indicated by Roman numbers I and II are assigned to the SPP, and a reflection of crystalline CHOL is indicated with an asterisk. (A) Diffraction pattern of the equimolar SCS (B) Diffraction pattern of the RXLI model. Broader reflections are located in the center of the ring at the same position as the first and second order of the SPP, indicating an oriented but more disordered additional phase. The intensity of the CHOL reflection is also strongly reduced.

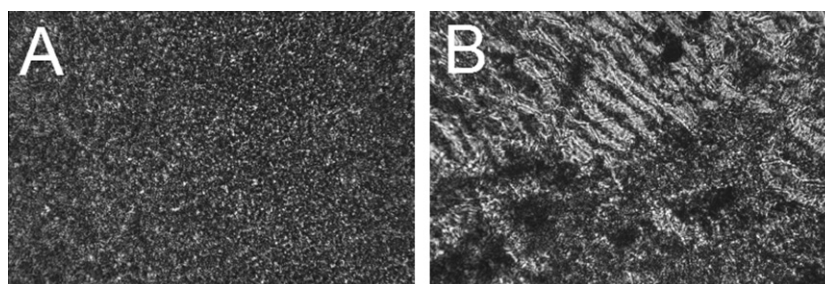


**Fig. 6.** Polarization microscopy images using a 40 $\times$  magnification. (A) Equimolar SCS, displaying a uniform pattern of small domains (B) The RXLI SCS, displaying large irregularly shaped domains.

and examined the equimolar and RXLI SCS also under a polarization microscope. When examining the two-dimensional detector image of the RXLI model, we observed that the increased level of  $\text{ChSO}_4$  induces a well-oriented but broad reflection, close to the position of the first order of the SPP, see Fig. 5. Also higher order broad reflections of this phase are observed. This indicates that an additional phase is present in the SCS. The less sharp reflections suggest a less ordered phase, which may account for the increased permeability. When further examining the RXLI model under a polarization microscope, we observed large patches that are absent in the equimolar SCS, see Fig. 6, confirming that an additional phase is formed by supplementing  $\text{ChSO}_4$ .

In conclusion, in our studies, two SCS models showed a significant change in BA steady-state flux; an excess of crystalline CHOL lead to a decreased steady-state flux, while an excess of  $\text{ChSO}_4$ , as observed in X-linked ichthyosis, led to an increase in the BA steady-state flux. While phase-separated CHOL is crystalline and therefore possibly difficult to penetrate, there is some evidence that the additional phase induced by  $\text{ChSO}_4$  is less ordered in nature accounting for the increased permeability. A change in CER:CHOL:FFA ratio in psoriasis skin and an increase in the CER EOS-oleate/CER EOS-linoleate ratio in dry skin may not be responsible for the impaired skin barrier function in vivo.

## Acknowledgments

This work was supported by a Grant from the Technology Foundation STW (LGP 7503). We thank the company Cosmoferm B.V. (Evonik) for the provision of the ceramides and the Netherlands Organization for Scientific Research (NWO) for the provision of beam time at the ESRF. Furthermore, we thank the personnel at the DUBBLE beam line at the ESRF for their support with the

X-ray measurements. Finally, we thank Dr. Maria Ponec for valuable discussions on the permeability studies.

## References

- [1] O. Simonetti, A.J. Hoogstraate, W. Bialik, J.A. Kempenaar, A.H. Schrijvers, H.E. Bodde, M. Ponec, Visualization of diffusion pathways across the stratum corneum of native and in-vitro-reconstructed epidermis by confocal laser scanning microscopy, *Arch. Dermatol. Res.* 287 (1995) 465–473.
- [2] Y. Masukawa, H. Narita, E. Shimizu, N. Kondo, Y. Sugai, T. Oba, R. Homma, J. Ishikawa, Y. Takagi, T. Kitahara, Y. Takema, K. Kita, Characterization of overall ceramide species in human stratum corneum, *J. Lipid Res.* 49 (2008) 1466–1476.
- [3] M. Ponec, A. Weerheim, P. Lankhorst, P. Wertz, New acylceramide in native and reconstructed epidermis, *J. Invest. Dermatol.* 120 (2003) 581–588.
- [4] K.J. Robson, M.E. Stewart, S. Michelsen, N.D. Lazo, D.T. Downing, 6-Hydroxy-4-sphingenine in human epidermal ceramides, *J. Lipid Res.* 35 (1994) 2060–2068.
- [5] M.E. Stewart, D.T. Downing, A new 6-hydroxy-4-sphingenine-containing ceramide in human skin, *J. Lipid Res.* 40 (1999) 1434–1439.
- [6] P.W. Wertz, M.C. Miethke, S.A. Long, J.S. Strauss, D.T. Downing, The composition of the ceramides from human stratum corneum and from comedones, *J. Invest. Dermatol.* 84 (1985) 410–412.
- [7] J.A. Bouwstra, G.S. Gooris, W. Bras, D.T. Downing, Lipid organization in pig stratum corneum, *J. Lipid Res.* 36 (1995) 685–695.
- [8] J.A. Bouwstra, G.S. Gooris, J.A. van der Spek, W. Bras, Structural investigations of human stratum corneum by small-angle X-ray scattering, *J. Invest. Dermatol.* 97 (1991) 1005–1012.
- [9] J.A. Bouwstra, G.S. Gooris, F.E. Dubbelaar, M. Ponec, Phase behavior of lipid mixtures based on human ceramides: coexistence of crystalline and liquid phases, *J. Lipid Res.* 42 (2001) 1759–1770.
- [10] J.A. Bouwstra, G.S. Gooris, F.E. Dubbelaar, M. Ponec, Phase behavior of stratum corneum lipid mixtures based on human ceramides: the role of natural and synthetic ceramide 1, *J. Invest. Dermatol.* 118 (2002) 606–617.
- [11] J. Bouwstra, G. Gooris, M. Ponec, The lipid organisation of the skin barrier: liquid and crystalline domains coexist in lamellar phases, *J. Biol. Phys.* 28 (2002) 211–223.
- [12] I. Hatta, N. Ohta, K. Inoue, N. Yagi, Coexistence of two domains in intercellular lipid matrix of stratum corneum, *Biochim. Biophys. Acta* 1758 (2006) 1830–1836.

- [13] S.H. White, D. Mirejovsky, G.I. King, Structure of lamellar lipid domains and corneocyte envelopes of murine stratum corneum. An X-ray diffraction study, *Biochemistry* 27 (1988) 3725–3732.
- [14] P. Wertz, *Epidermal lipids*, in: L.A. Goldsmith (Ed.), *Physiology, Biochemistry and Molecular Biology of the Skin*, Oxford University Press, Oxford, 1991, pp. 205–235.
- [15] M.L. Williams, P.M. Elias, Stratum corneum lipids in disorders of cornification: increased cholesterol sulfate content of stratum corneum in recessive X-linked ichthyosis, *J. Clin. Invest.* 68 (1981) 1404–1410.
- [16] P.M. Elias, M.L. Williams, M.E. Maloney, J.A. Bonifas, B.E. Brown, S. Grayson, E.H. Epstein Jr., Stratum corneum lipids in disorders of cornification. Steroid sulfatase and cholesterol sulfate in normal desquamation and the pathogenesis of recessive X-linked ichthyosis, *J Clin Invest* 74 (1984) 1414–1421.
- [17] S. Motta, S. Sesana, R. Ghidoni, M. Monti, Content of the different lipid classes in psoriatic scale, *Arch. Dermatol. Res.* 287 (1995) 691–694.
- [18] J. Rogers, C. Harding, A. Mayo, J. Banks, A. Rawlings, Stratum corneum lipids: the effect of ageing and the seasons, *Arch. Dermatol. Res.* 288 (1996) 765–770.
- [19] E. Zettersten, M.Q. Man, J. Sato, M. Denda, A. Farrell, R. Ghadially, M.L. Williams, K.R. Feingold, P.M. Elias, Recessive X-linked ichthyosis: role of cholesterol-sulfate accumulation in the barrier abnormality, *J. Invest. Dermatol.* 111 (1998) 784–790.
- [20] T.J. McIntosh, Organization of skin stratum corneum extracellular lamellae: diffraction evidence for asymmetric distribution of cholesterol, *Biophys. J.* 85 (2003) 1675–1681.
- [21] D. Kuempel, D.C. Swartzendruber, C.A. Squier, P.W. Wertz, In vitro reconstitution of stratum corneum lipid lamellae, *Biochim. Biophys. Acta* 1372 (1998) 135–140.
- [22] J.A. Bouwstra, G.S. Gooris, K. Cheng, A. Weerheim, W. Bras, M. Poncet, Phase behavior of isolated skin lipids, *J. Lipid Res.* 37 (1996) 999–1011.
- [23] M. de Jager, W. Groenink, R. Bielsa i Guivernau, E. Andersson, N. Angelova, M. Poncet, J. Bouwstra, A novel in vitro percutaneous penetration model: evaluation of barrier properties with p-aminobenzoic acid and two of its derivatives, *Pharm. Res.* 23 (2006) 951–960.
- [24] M. de Jager, W. Groenink, J. van der Spek, C. Janmaat, G. Gooris, M. Poncet, J. Bouwstra, Preparation and characterization of a stratum corneum substitute for in vitro percutaneous penetration studies, *Biochim. Biophys. Acta* 1758 (2006) 636–644.
- [25] D. Groen, G.S. Gooris, M. Poncet, J.A. Bouwstra, Two new methods for preparing a unique stratum corneum substitute, *Biochim. Biophys. Acta* 1778 (2008) 2421–2429.
- [26] D. Groen, D.S. Poole, G.S. Gooris, J.A. Bouwstra, Is an orthorhombic lateral packing and a proper lamellar organization important for the skin barrier function?, *Biochim Biophys. Acta* 1808 (2010) 1529–1537.
- [27] S. Motta, M. Monti, S. Sesana, R. Caputo, S. Carelli, R. Ghidoni, Ceramide composition of the psoriatic scale, *Biochim. Biophys. Acta* 1182 (1993) 147–151.
- [28] G.S. Gooris, J.A. Bouwstra, Infrared spectroscopic study of stratum corneum model membranes prepared from human ceramides, cholesterol, and fatty acids, *Biophys. J.* 92 (2007) 2785–2795.
- [29] R.G. Snyder, S.L. Hsu, S. Krimm, Vibrational-spectra in C–H stretching region and structure of polymethylene chain, *Spectrochim. Acta Part A – Mol. Biomol. Spectrosc.* 34 (1978) 395–406.
- [30] P. Wolfangel, R. Lehnert, H.H. Meyer, K. Muller, FTIR studies of phospholipid membranes containing monoacylenic acyl chains, *Phys. Chem. Chem. Phys.* 1 (1999) 4833–4841.
- [31] R.G. Snyder, Vibrational spectra of crystalline N-paraffins. 1. Methylene rocking and wagging modes, *J. Mol. Spectrosc.* 4 (1960) 411–434.
- [32] D.J. Moore, M.E. Rerek, R. Mendelsohn, Lipid domains and orthorhombic phases in model stratum corneum: Evidence from Fourier transform infrared spectroscopy studies, *Biochem. Biophys. Res. Commun.* 231 (1997) 797–801.
- [33] A. Conti, J. Rogers, P. Verdejo, C.R. Harding, A.V. Rawlings, Seasonal influences on stratum corneum ceramide 1 fatty acids and the influence of topical essential fatty acids, *Int. J. Cosmet. Sci.* 18 (1996) 1–12.
- [34] M.E. Rerek, H. Chen, B. Markovic, D. van Wyck, P. Garidel, R. Mendelsohn, D.J. Moore, Phytosphingosine and sphingosine ceramide headgroup hydrogen bonding: structural insights through thermotropic hydrogen/deuterium exchange, *J. Phys. Chem. B* 105 (2001) 9355–9362.
- [35] M. Janssens, G.S. Gooris, J.A. Bouwstra, Infrared spectroscopy studies of mixtures prepared with synthetic ceramides varying in head group architecture: coexistence of liquid and crystalline phases, *Biochim. Biophys. Acta* 1788 (2009) 732–742.
- [36] J.C. Garson, J. Doucet, J.L. Leveque, G. Tsoucaris, Oriented structure in human stratum corneum revealed by X-ray diffraction, *J. Invest. Dermatol.* 96 (1991) 43–49.
- [37] J.C. Gomez-Fernandez, J. Villalain, The use of FT-IR for quantitative studies of the apparent  $pK_a$  of lipid carboxyl groups and the dehydration degree of the phosphate group of phospholipids, *Chem. Phys. Lipids* 96 (1998) 41–52.
- [38] A.V. Rawlings, J. Hope, J. Rogers, A.M. Mayo, I.R. Scott, Mechanisms of desquamation: new insights into dry flaky skin conditions, in: *Proceedings of the 17th IFSCC International Congress*, vol. 2, 1992, pp. 865–880.
- [39] A.V. Rawlings, A. Watkinson, J. Rogers, A.M. Mayo, J. Hope, I.R. Scott, Abnormalities in stratum-corneum structure, lipid-composition, and desmosome degradation in soap-induced winter xerosis, *J. Soc. Cosmet. Chem.* 45 (1994) 203–220.
- [40] J. Marks, S. Rogers, B. Chadkirk, S. Shuster, Clearance of chronic plaque psoriasis by anthralin – subjective and objective assessment and comparison with photochemotherapy, *Brit. J. Dermatol.* 105 (1981) 96–99.
- [41] J.A. Bouwstra, G.S. Gooris, F.E. Dubbelaar, M. Poncet, Cholesterol sulfate and calcium affect stratum corneum lipid organization over a wide temperature range, *J. Lipid Res.* 40 (1999) 2303–2312.
- [42] J.A. Bouwstra, G.S. Gooris, F.E. Dubbelaar, A.M. Weerheim, M. Poncet, pH, cholesterol sulfate, and fatty acids affect the stratum corneum lipid organization, *J. Invest. Dermatol. Symp. Proc.* 3 (1998) 69–74.